Impaired BCAA catabolism during adipocyte differentiation decreases glycolytic flux

Courtney R. Green[1,2,5], Karl A. Wessendorf-Rodriguez[1,2], Rory Turner[3], Justin D. Hover[2], Anne N. Murphy[4], Christian M. Metallo[1,2]*, Martina Wallace[3]*

Affiliations:

1. Molecular and Cellular Biology Laboratory, Salk Institute for Biological Studies, 10010 N. Torrey Pines Rd., La Jolla, CA, USA 92037
2. Department of Bioengineering, University of California, San Diego, 9500 Gilman Drive, La Jolla, CA, USA 92093
3. School of Agriculture and Food Science, University College Dublin, Belfield, Dublin 4, Ireland
4. Department of Pharmacology, University of California, San Diego, 9500 Gilman Drive, La Jolla, CA, USA 92093
5. Present address: Dexcom, Inc., 6340 Sequence Dr., San Diego, CA, USA 92121

* To whom correspondence should be addressed:

Martina Wallace (martina.wallace@ucd.ie, +353 1 7166932) and Christian M. Metallo (metallo@salk.edu +1 858 453 4100 x1293)

Abstract

Objective: Adipocytes upregulate branched-chain amino acid (BCAA) catabolism during differentiation, but the downstream metabolic and biological impacts of this induction remain

unclear. Here we sought to understand how BCAA catabolism supports intermediary metabolism and function in cultured adipocytes.

Methods: Using CRISPR/Cas9 gene-editing, we generated 3T3-L1 pre-adipocytes deficient in either branched-chain ketoacid dehydrogenase, subunit alpha (*Bckdha*) or acyl-CoA dehydrogenase 8 (*Acad8*), which predominantly metabolizes valine-derived isobutyryl-CoA, and examined their metabolism after differentiation. We performed stable-isotope tracing and mass spectrometry, developed a ^{13}C metabolic flux analysis (^{13}C-MFA) model incorporating central carbon metabolism and lipid biosynthesis, and performed RNA-sequencing to further explore functional changes.

Results: Generation of polyclonal cultures deficient in *Bckdha* resulted in a 90%+ decrease in [U-$^{13}C_6$]leucine labeling in citrate in differentiated adipocytes ($p<0.001$). Lipid droplet accumulation and mRNA levels of key markers of adipocyte differentiation were unaffected by *Bckdha* deficiency; however, gene set enrichment analysis (GSEA) indicated adipogenesis and glycolysis were the primary downregulated pathways in these cells. *Bckdha*-deficient adipocytes had decreased glucose uptake ($p<0.05$), glycolytic flux ($p<0.05$), and increased glutamine contribution to the TCA cycle ($p<0.05$). These findings were supported by reduced lactate secretion ($p<0.001$) and oxygen consumption rates ($p<0.05$) and correlated with the transcriptional changes observed in adipocytes. Total *de novo* fatty acid synthesis flux was maintained but levels of odd-chain fatty acids and branched-chain fatty acids were reduced, as was the C16:1/C16:0 ratio. ^{13}C-MFA confirmed these changes and highlighted the complex relationship between the TCA cycle, BCAA catabolism, and mitochondrial respiration. Finally, *Acad8* deficiency resulted in far fewer differentially expressed genes compared to *Bckdha* deficiency and milder metabolic changes overall.

Conclusions: These findings highlight key metabolic and transcriptional changes that occur due to *Bckdha* deficiency in adipocytes and identify important links between BCAA catabolism, glycolytic flux, and respiration.

Highlights:

- *Bckdha* deficiency reduced glycolysis and lactate secretion in adipocytes
- Pyruvate and glutamine contribution to TCA metabolism and acetyl-CoA increased
- *de novo* fatty acid synthesis flux was maintained but fatty acid diversity decreased
- RNA-seq data highlighted regulation of genes in glycolysis, adipogenesis, and EMT
- *Acad8* deficiency resulted in fewer altered transcripts and milder metabolic changes

Introduction

The branched-chain amino acids (BCAAs) leucine, isoleucine, and valine are essential amino acids catabolized by a series of mitochondrial enzymes to acetyl-CoA and propionyl-CoA (PropCoA). While diverse tissues use this pathway for energy generation, signaling, and biosynthesis (*1, 2*), adipose tissue is increasingly appreciated as an important contributor to BCAA homeostasis (*3-7*). This pathway is upregulated during the initial stages of adipocyte differentiation (*6-12*) and is highly active in brown adipose tissue where BCAA catabolism is required to maintain thermogenesis in mice (*5*). Catabolism of BCAAs in adipocytes is initiated by mitochondrial BCAT2, which transfers the amino nitrogen to α-ketoglutarate yielding glutamate and a corresponding branched-chain α-keto acid (BCKA). These BCKAs are subsequently oxidized by the branched-chain ketoacid dehydrogenase (BCKD) complex, a highly regulated, rate-limiting step in BCAA catabolism, which decarboxylates the BCKA, covalently adds a coenzyme A moiety, and yields a short branched-chain fatty acyl-CoA (SBCFA-CoA). A series of enzymatic steps further catabolize SBCFA-CoAs to acetyl-CoA and propionyl-CoA, with the latter serving as an anaplerotic substrate for the tricarboxylic acid cycle upon conversion to methylmalonyl-CoA in an adenosylcobalamin-dependent reaction. Alternatively, SBCFA-CoAs and other pathway intermediates are exported to the cytosol to act as signaling molecules or substrates for fatty acid synthase (FASN), which results in formation of iso- or anteiso-monomethyl branched-chain fatty acids (BCFAs) (*13-16*).

Elevated circulating BCAAs are emerging as a hallmark of metabolic syndrome (*17-19*) and insulin resistance and obesity are associated with systemic dysregulation of BCAA metabolism (*1*). Transcriptional and proteomic studies of white adipose tissue in humans indicate obesity and

insulin resistance significantly suppress BCAA catabolism in this tissue (*12, 20*). *In vitro* studies have shown that hypoxic stress potently downregulates flux through BCAA catabolism in adipocytes (*13*) and recent studies in humans found BCAA catabolic gene expression positively correlates with oxygen tension in humans (*21*). This indicates obesity-induced hypoxia may mediate the observed defects in BCAA catabolism in obese adipose tissue. Given the plasticity of adipose tissue (*22, 23*) with an estimated 10% annual turnover of adipocytes (*24*), there is a need to understand how suppression of BCAA catabolism during differentiation due to the obese microenvironment may impact differentiation and function. Previous *in vitro* studies have found that shRNA mediated knockdown of branched-chain ketoacid dehydrogenase, subunit alpha (*Bckdha*) (*10*), the leucine catabolic enzyme methylcrotonoyl-CoA carboxylase 1 (*Mccc1*) (*6*) or siRNA-mediated knockdown of 3-hydroxyisobutyryl-CoA hydrolase (*Hibch*) (*25*) throughout differentiation decreased lipid accumulation indicating impaired differentiation. *In vivo*, knockout of *Bcat2* in white adipocytes induces interscapular white adipose tissue (iWAT) browning (*15*) whereas disruption of BCAA catabolism in brown adipose tissue via knockout of the mitochondrial BCAA transporter *Slc25a44* or *Bckdha* impairs thermogenesis (*5, 26*). Collectively, these data indicate altered BCAA catabolism significantly impacts adipocyte function but a comprehensive assessment of how this impacts flux through other pathways in central carbon metabolism is lacking.

Defects in BCAA catabolism also define certain Mendelian disorders such as maple syrup urine disease (MSUD) which present with diverse neurological and growth phenotypes (*27, 28*). For example, MSUD patients have very little BCKDH complex activity, which results in elevated levels of BCAAs and BCKAs (*29*). Left untreated, MSUD can cause neurological dysfunction and

focal brain injury that results in failure to thrive, seizure, coma, and death within the first weeks of life. Dietary interventions are efficacious for some patients, but chronic neuropsychological problems can persist (*29-33*). Inborn errors of metabolism also exist in the Acad family of enzymes, such as isobutyryl-CoA dehydrogenase deficiency (IBDD). IBDD is caused by mutations in *Acad8* which prevents complete valine catabolism (*34*, *35*). In contrast to MSUD, IBDD is often asymptomatic in infants and can remain undiagnosed until a major health event occurs (*36*). As such, key questions remain regarding the biochemical drivers of pathophysiology of such organic acidemias, which could result from changes in the abundance of BCAAs, BCKAs, post-translational modifications, or lipids.

Here we sought to functionally interrogate the BCAA pathway by engineering cultured 3T3-L1 adipocytes to be deficient in *Bckdha* or *Acad8* genes using CRISPR/Cas9. Using stable isotope tracing, mass spectrometry, transcriptomics, and metabolic flux analysis (MFA) modeling, we demonstrate that impairment of BCAA catabolism results in decreased glycolytic flux, lactate secretion, and oxygen consumption. Flux through fatty acid synthase, however, is maintained and this is supported by increased glutamine utilization and increased entry of pyruvate into the TCA cycle. Although lipid droplet accumulation and expression of key adipocyte differentiation markers is not impacted by *Bckdha* or *Acad8* deficiency, gene set enrichment analysis of RNAseq data reveal downregulation of genes associated with adipogenesis, hypoxia, and glycolysis indicating more subtle changes in differentiation and function. In addition, comparison of *Acad8* and *Bckdha* deficiency revealed that *Bckdha* deficiency leads to far more significantly altered pathways at both the transcriptional and metabolic level. These cell metabolism studies provide a

detailed roadmap for exploring and understanding the BCAA catabolic pathway and its regulation in adipocytes.

Results

Generation and validation of Bckdha-*deficient adipocyte cultures*

To explore the impact of compromised BCAA catabolism in adipocytes we generated polyclonal cultures of 3T3-L1 pre-adipocytes lacking *Bckdha* using CRISPR/Cas9 (single-guide (sg) Control and *Bckdha*) (Fig 1A). Lipid accumulation appeared unaffected (Fig 1B) and *Bckdha* knockdown was further confirmed with a 90%+ decrease in [U-$^{13}C_6$]leucine labeling to citrate (Fig. 1C). The expression of key adipocyte mRNA differentiation markers was largely unchanged in these polyclonal cultures (Fig. 1D), indicating a minimal impact on differentiation efficiency. However, higher BCAA abundances and an elevated α-ketoisocaproate (KIC)/Leucine ratio were seen in *Bckdha*-deficient adipocytes (Fig. 1E & Supp. Fig. 1A). Uptake of all BCAAs was also significantly reduced (Fig. 1F). As BCAA catabolism can supply nitrogen for amino acid synthesis, we also quantified the net uptake, secretion, or biosynthesis of non-essential amino acids from [U-$^{13}C_6$]glucose. These rates were largely unchanged in *Bckdha*-deficient adipocytes under the nitrogen-replete conditions tested here (Supp. Fig. 1B-C).

To examine the impact of *Bckdha* deficiency on gene expression in adipocytes, we performed RNAseq on our polyclonal cell populations. We found 887 genes that were significantly differentially expressed (Fig. 2A). These genes included *Scd1* and *Scd2* as well as *Sema3g*, an adipokine recently shown to be essential for adipogenesis and lipogenesis (*37*). To categorize these differentially expressed genes further, we used WEB-based gene set analysis toolkit (WebGestalt)

to perform gene set enrichment analysis (GSEA) with the KEGG pathway functional database. We found seven significantly altered pathways with FDR <0.05, which comprised key functional, metabolic, and signaling pathways relevant for adipocyte function, including oxidative phosphorylation, thermogenesis, glycolysis, HIF-1 signaling, and AMPK signaling (Fig. 2B). We also performed GSEA using the MSigDB biological processes hallmark gene sets database. Notably, adipogenesis was the most downregulated pathway in this analysis, and epithelial-to-mesenchymal transition (EMT) was significantly upregulated (Supp. Fig. 2A), further suggesting that *Bckdha* deficiency impacts cellular differentiation state and broader signaling to some extent. Collectively, these results point to an overall downregulation of adipocyte metabolism and impaired function despite the lack of obvious visual signs or consistent reduction in core differentiation markers as measured by qPCR (Fig. 1D). To complement these broad characterizations of secreted metabolites and pathway transcription in *Bckdha*-deficient adipocytes, we next quantified pathway fluxes in greater detail to better understand how the adipocyte metabolic network was rewired in this setting.

Bckdha-*deficient adipocytes reprogram intermediary metabolism and bioenergetics*

Glycolysis/gluconeogenesis was one of the most downregulated pathways in our GSEA of *Bckdha*-deficient adipocytes. In addition, decreased alanine levels (Fig. 1E) indicated a potential reprogramming of glucose metabolism and alternative usage of pyruvate (Fig. 3A). To explore these changes more directly, we quantified glycolytic rates and the lactate/pyruvate ratio in Control and *Bckdha*-deficient adipocytes. Glucose uptake decreased by up to ~25% (Fig. 3B) but we observed a ~50% decrease in lactate secretion in *Bckdha*-deficient adipocytes (Fig. 3C). Indeed, a reduction in the ratio of lactate secretion/glucose uptake (Fig. 3D) and lactate and pyruvate

abundances (Fig. 3E) further supported the reduction in glycolysis suggested by our RNAseq analysis.

Next, we sought to explore TCA metabolism in greater detail, as reduced BCAA catabolism could limit the supply of oxidative substrates supplying mitochondria and drive increased pyruvate oxidation to compensate. Interestingly, all TCA cycle intermediates were significantly decreased in *Bckdha*-deficient adipocytes (Fig. 4A). We also observed a consistent ~20% decrease in both the basal and maximal oxygen consumption rate (Fig. 4B), similar to results in brown adipocytes deficient in the mitochondrial BCAA transporter SLC25A44 (*5*). To determine how impaired BCAA catabolism impacts the use of other carbon sources, we traced adipocytes with [U-$^{13}C_6$]glucose and [U-$^{13}C_5$]glutamine and quantified isotope enrichment in TCA intermediates. Importantly, we observed a slight, but significant increase in mole percent enrichment (MPE) of citrate, α-ketoglutarate (aKG), and succinate from [U-$^{13}C_6$]glucose in *Bckdha*-deficient adipocytes (Fig. 4C), with relatively subtle differences in the isotopologue distribution of citrate (Supp. Fig. 2B). MPE from [U-$^{13}C_5$]glutamine was significantly higher in all TCA intermediates except succinate in *Bckdha*-deficient adipocytes (Fig. 4D). In both 3T3-L1 adipocytes and epididymal white adipose tissue (eWAT), leucine and valine alone contribute 3-8% to the total TCA cycle metabolite mole percent enrichment (Fig. 4E). Therefore, it is consistent that ablation of BCAA catabolism in adipocytes is marked by a reduction in mitochondrial respiration and compensatory increases in pyruvate and glutamine entry into the TCA cycle. Importantly, we saw no significant changes in mitochondrial DNA content in 3T3-L1 adipocytes lacking *Bckdha*, indicating that the reduction in respiration is likely not due to reduced mitochondrial number but rather their function (Supp. Fig. 2C).

Bckdha *deficiency alters lipogenic acetyl-CoA sourcing and FA diversity*

Bckdha deficiency prevents the formation of Prop-CoA and SBCFA-CoAs, which contribute to the synthesis of odd-chain fatty acids (OCFAs) and branched-chain fatty acids (BCFAs) (*9, 10, 13*). As expected, OCFAs and BCFAs were greatly decreased, while the proportion of even chain fatty acids was significantly increased in *Bckdha*-deficient adipocytes (Fig. 5A-B). Isotopomer spectral analysis (ISA) of palmitate labeling from [U-$^{13}C_6$]glucose demonstrated that the contribution of glucose/pyruvate oxidation to the lipogenic acetyl-CoA pool was also significantly increased (Fig. 5C), further highlighting the compensatory increase in glucose metabolism when BCAA catabolism is impaired. ISA modeling also revealed a decrease in newly synthesized OCFAs and a modest increase in the proportion of newly synthesized C16:0 (Fig. 5D). However, the total amount of newly synthesized fatty acids (accounting for both percentage of pool newly synthesized and molar amount of FA) remained unchanged in *Bckdha*-deficient adipocytes (Fig. 5E). These results indicate that central carbon metabolism is rewired to sustain FA synthesis (i.e. acetyl-CoA sourcing) and overall abundances.

RNAseq results also indicated that expression of the desaturase enzymes SCD1 and SCD2 was decreased in *Bckdha*-deficient adipocytes. To this end we calculated the desaturation index (ratio of monounsaturated to saturated FA) in each cell type. While the C18:1/C18:0 ratio was unchanged, the C16:1/C16:0 ratio was significantly decreased in *Bckdha*-deficient adipocytes indicating a decrease in C16:0 desaturation. As both C18:1 and C18:0 are derived more from uptake than synthesis (compared to C16:1 and C16:0), this difference likely reflects a decrease in desaturation activity that is buffered by import of C18:1 from serum in media (Fig. 5F).

MFA modeling of Bckdha-*deficient adipocytes*

To gain confidence in the above interpretations we incorporated data from Control and *Bckdha*-deficient adipocytes cultured with either [U-$^{13}C_6$]glucose, [U-$^{13}C_6$]leucine, or [U-$^{13}C_5$]valine for 48 hours into a MFA model using INCA (*38*). The network encompassed relevant reactions within glycolysis, TCA metabolism, BCAA oxidation, and fatty acid synthesis, with compartmentalization of several pathways included (Fig. 6A). The model incorporated isotope enrichment data for pyruvate, TCA cycle intermediates, intracellular and extracellular glutamine, intracellular glutamate, leucine, KIC, valine, and fatty acids C15:0, C16:0, and C17:0, as appropriate (Supplementary Table 1). Direct measurements of uptake and secretion fluxes for glucose, lactate, alanine, valine, leucine, glutamate, and glutamine were also included (Supplementary Table 2-3). The model predicts a significant decrease in glucose uptake and both lactate and alanine secretion (Fig 1E & Fig. 3B-C) in 3T3-L1 *Bckdha*-deficient adipocytes. On the other hand, *Bckdha*-deficient adipocytes exhibited a marked increase in pyruvate dehydrogenase (PDH) flux as well as mitochondrial pyruvate cycling, which is consistent with the observed reduction in acetyl-CoA derived from leucine/isoleucine catabolism. We also included FA synthesis in this model, which trended higher but was not significantly different between the cell types despite the noted shift toward palmitate over OCFA and BCFA synthesis in *Bckdha*-deficient adipocytes. Notably, anaplerotic flux of BCAAs to succinyl-CoA was low in all cells, presumably due to the lack of vitamin B12 present in these cultures (*10*). This shift in carbon balancing from BCAA oxidation to glucose/pyruvate oxidation resulted in the model predicting an increase in oxidative TCA cycle flux. Indeed, glutamine contribution to the TCA cycle was also estimated to be increased in *Bckdha*-deficient adipocytes, which also exhibited higher rates of exchange between glutamate and aKG. These results are in agreement with our independent results using

[U-$^{13}C_5$]glutamine as a tracer (Fig. 4D), which were not incorporated into the model due to the high exchange with medium glutamine. Additionally, the model predicted an increase in the uptake (56 nmol/well/h vs 45 nmol/well/h) and secretion (43 nmol/well/h vs 39 nmol/well/h) of glutamine, consistent with the increase in labeled glutamine from the [U-$^{13}C_6$]glucose and decrease in total glutamine in the spent media. These findings highlight the broad impact of *Bckdha* deficiency on nitrogen and amino acid metabolism (*39*).

Acad8 *deficiency impacts anaplerosis and iso-C16:0 BCFA accumulation*

In addition to *Bckdha* deficiency, which prevents catabolism of all three BCAAs and downstream pathways, we also investigated the phenotype of adipocytes deficient in *Acad8*, which catalyzes the oxidation of valine-derived isobutyryl-CoA (and thus only blocks valine catabolism). ACAD8 protein knockdown (Fig. 7A) did not grossly affect lipid accumulation or adipogenic differentiation (Fig. 7B), as observed with *Bckdha* deficiency (Fig. 1B). However, RNAseq analysis of these *Acad8*-deficient adipocytes found only 65 differentially expressed genes ($q<0.05$) (Fig. 7C), much less than the 887 genes observed in our analysis of *Bckdha*-deficient adipocytes (Fig. 2A). Furthermore, *Acad8* deficiency did not consistently alter TCA cycle intermediate levels (Fig. 7D) or citrate labeling from [U-$^{13}C_6$]glucose (Fig. 7E). While *Acad8* deficiency reduced OCFA levels by about 20% and dramatically increased iso-C16:0 abundance, other fatty acids were not affected (Fig. 7F-G), similar to results obtained with shRNA knockdown (*13*). Overall, these results suggest that *Acad8* deficiency elicits more moderate effects compared to *Bckdha* deficiency, which mirrors the relatively minimal phenotype in humans with IBDD compared to MSUD/*Bckdha* deficiency. Collectively, our studies in cultured adipocytes highlight key pathway alterations that occur when BCAA catabolism is compromised.

Discussion

Here we explored how central carbon metabolism is rebalanced in the absence of BCAA or valine catabolism in cultured 3T3-L1 adipocytes. Upon knockdown of *Bckdha* using CRISPR/Cas9, adipocytes maintain fatty acid biosynthetic flux by increasing pyruvate oxidation, glutamine utilization and consequently TCA flux. Notably, glycolysis, oxygen consumption and fatty acid diversity are reduced as a consequence of decreased BCAA catabolism. Overall, our results suggest that adipocytes retain adequate metabolic plasticity to support their biosynthetic demands in the absence of BCKDH activity.

Our results suggest that decreased BCKDH activity in adipocytes impacts glycolysis and glucose oxidation in distinct ways. In order to maintain *de novo* lipogenesis in the absence of BCAA catabolism, which can account for 30% lipogenic acetyl-CoA (*10, 13*), cells increase reliance on acetyl-CoA generation from glucose. To support this flux, adipocytes increase pyruvate transport into the mitochondria and oxidation by PDH. This increased utilization of pyruvate for acetyl-CoA does not lead to increased glycolysis. Instead, glycolytic flux is decreased and lactate secretion is significantly suppressed to enable increased channeling of pyruvate to the mitochondria. Although we could not resolve cytosolic from mitochondrial malic enzyme flux, these results highlight the importance of pyruvate cycling, as cytosolic malic enzyme is a major producer of lipogenic NADPH in adipocytes (*40, 41*). Interestingly, our MFA model estimated oxidative TCA cycle flux to be higher in *Bckdha*-deficient adipocytes (Fig. 6A), despite the reduced oxygen consumption measured independently in these cells (Fig. 4B). Various factors could account for this difference, including an expected increase in the NADH/$FADH_2$ ratio generated by pyruvate- and glutamine-driven TCA flux versus BCAA catabolism. The increased NADH/$FADH_2$ ratio will

increase flux through NADH-driven complex I of the electron transport chain. As the P/O ratio (ATP produced per oxygen atom reduced) of NADH is greater than that of $FADH_2$, the cell may be able to meet ATP demands using less oxygen. This potential shift to Complex I-driven respiration is also reflected in the RNAseq gene expression results, where *mt-Nd4,* encoding a complex I subunit, is one of the most upregulated genes in the *Bckdha*-deficient cells.

Lipid droplet accumulation was not impacted in our polyclonal *Bckdha*-deficient adipocytes, which contrasts our prior results targeting *Bckdha* using shRNA (*10*) and those of others utilizing shRNA or siRNA to alter MCCC1 and HIBCH levels (*6, 25*). However, RNAseq analysis found that adipogenesis was the most downregulated pathway using the molecular signatures database. Increased expression of genes associated with epithelial-to-mesenchymal transition also indicated impaired cellular functional state and differentiation (Supp. Fig. 2B). While our analysis focused on metabolic changes with BCKDH deficiency, our RNAseq results indicate that it may also have broader impacts on cell identity and further studies are needed.

These cell-based studies provide insights into the broader metabolic changes associated with organic acidemias of the BCAA catabolic pathway, particularly in adipose tissue. Many of these changes are likely to result directly due to a decrease in BCAA-derived carbon and associated reducing equivalents generated from their catabolism. However, *Bckdha* deficiency can also result in elevated BCKAs, and several studies implicate elevated BCKAs but not BCAAs in alterations such as impaired insulin signaling (*42*), reduced TCA cycle intermediate abundances (*43*), and reduced mitochondrial OCR (*44, 45*). Notably, *Bckdha* deficiency induced much broader changes in metabolism and gene expression than *Acad8* deficiency, where valine-mediated anaplerosis was

reduced and iso-C16:0 BCFA increased dramatically without grossly altering intermediary metabolism or gene expression. While aberrant accumulation of BCFAs can cause deleterious effects (*46*), these results generally correlate with the higher severity of symptoms in patients with MSUD versus IBDD (*28*). However, endogenous production of BCFAs is blocked in *Bckdha*-deficient adipocytes, similar to reductions observed in obese adipose tissue (*13, 47, 48*) and circulating levels in children with fatty liver (*49*). BCFAs are incorporated into diverse lipid species, which could influence membrane fluidity and associated signaling or metabolic processes (*13, 50-52*). Collectively, these results further highlight the diverse metabolic pathways impacted downstream of BCAA catabolism in adipocytes that warrant further exploration.

Acknowledgments

We thank all members of the Metallo laboratory for support and helpful discussions. This study was supported, in part, by US National Institutes of Health (NIH) grants R01CA234245 (C.M.M.). M.W. and R.T. are supported by an Ad Astra fellowship. This publication includes data generated at the UC San Diego IGM Genomics Center utilizing an Illumina NovaSeq 6000 that was purchased with funding from a National Institutes of Health SIG grant (#S10 OD026929). We would also like to thank Dr. Yan Wu for guidance in RNAseq analysis.

Author Contributions

C.R.G., M.W., and C.M.M. conceived and designed the study. K.W.-R. performed MFA analysis. C.R.G. conducted RNAseq analysis and KEGG pathway analysis. R.T. and M.W. conducted MSigDB-based RNAseq analysis. M.W. performed *in vivo* tracing studies. C.R.G. and J.D.H. carried out gene expression analysis. J.D.H. assisted with stable-isotope tracing

experiments and GC-MS analysis. A.N.M. provided Seahorse equipment and related training and advice. C.R.G. performed all other experiments. C.R.G., M.W., and C.M.M. wrote the paper with input from all authors.

Materials & Methods

Cell Culture & Differentiation

All reagents were purchased from Sigma-Aldrich unless otherwise noted. All media and sera were purchased from Life Technologies unless otherwise stated. Mouse 3T3-L1 pre-adipocytes were provided by Prof. Alan Saltiel and cultured in high glucose Dulbecco's modified Eagle medium (DMEM) (Life Technologies) supplemented with 10% bovine calf serum (BCS) below 70% confluence. Cells were regularly screened for mycoplasma contamination. For differentiation, 10,000 cells/well were seeded onto 12-well plates and allowed to reach confluence (termed Day -1). On Day 0, differentiation was induced with 0.5 mM 3-isobutyl-1-methylxanthine (IBMX), 0.25 μM dexamethasone, and 1 μg/ml insulin in DMEM containing 10% FBS. Medium was changed on Day 3 to DMEM + 10% FBS with 1 μg/ml insulin. Day 6, and thereafter, DMEM + 10% FBS was used.

Isotope tracing was carried out 7d post-induction of differentiation. Cells were incubated in custom DMEM (Hyclone) in which the metabolite specified was replaced with the ^{13}C- or ^{2}H-labeled version for 24h unless otherwise specified. Fatty acids were then either calculated as percent total fatty acids and normalized to control conditions or normalized to [$^{2}H_{31}$]Palmitate internal standard and normalized to control conditions.

Generation of lentiviral CRISPR/Cas9 KO 3T3-L1 adipocytes

Control, Bckdha, and Acad8 target sequences (Supplementary Table 4) were cloned into the lentiCRISPRv2 plasmid, a gift from Feng Zhang (Addgene plasmid #52961) (*53*). For lentivirus production, 2-2.5 million HEK293FT cells were placed in 10cm tissue culture plates in 2 mL of DMEM (containing 1% penicillin/streptomycin, 10% FBS). 24h later, transfection was performed using Lipofectamine 3000 (Invitrogen) with 1.3µg VSV.G/PMD2.G, 5.3µg of lenti-gag/pol/PCMVR8.2 and 4µg of lentiviral vector. Lentivirus-containing supernatants were harvested 48 and 72h later, combined, and concentrated using Amicon Ultra-15 centrifugal filters, 100,000 NMWL (Millipore) following the manufacturer's protocol. 3T3-L1 pre-adipocytes were infected with 7µL of virus in 2mL of medium containing 7.5µg of polybrene in a 35mm cell culture dish. Media was changed the following day and allowed to recover for 24h. Selection was performed using 2µg/mL puromycin. Cells were then plated to 12-well plates for differentiation as described above. Puromycin was removed from the medium beginning on day 0 of differentiation.

Western Blots

3T3-L1 adipocytes were lysed in ice-cold RIPA buffer with 1x protease inhibitor (Sigma-Aldrich). 25µg total protein was separated on a 10% SDS-PAGE gel for BCKDHA and β-actin, while 50µg total protein was loaded for ACAD8. The proteins were transferred to a nitrocellulose membrane and immunoblotted with anti-BCKDHA (Novus Biologicals NBP1-79616) (1:2,500 dilution), anti-β-Actin (Cell Signaling 4970S) (1:10,000), anti-ACAD8 (Aviva Systems Biology OAAB06085) (1:1,000 dilution). Specific signal was detected with horseradish peroxidase-conjugated secondary antibody goat anti-rabbit (1:2,500-1:10,000) using SuperSignal West Pico

Chemiluminescent Substrate (Thermo Scientific) and developed using Blue Devil Autoradiography film (Genesee Scientific) or Bio-Rad Chemidoc XRS+ Imaging device.

Extraction of metabolites for GC-MS analysis

For cell culture, polar metabolites and fatty acids were extracted using methanol/water/chloroform with [$^{2}H_{31}$]palmitate and norvaline as lipid and polar internal standards, respectively, and analyzed as previously described (*54*). Briefly, cells were washed twice with saline, quenched with -80C methanol and 4C water containing norvaline, scraped into Eppendorfs, and extracted with chloroform containing [$^{2}H_{31}$]Palmitate. After centrifugation, phases are dried separately. Samples are stored at -20C before analysis by GC-MS.

GC-MS analysis

Dried polar metabolites were derivatized in 2% (w/v) methoxyamine hydrochloride (Thermo Scientific) in pyridine and incubated at 37°C for 60 min. Samples were then silylated with N-tertbutyldimethylsilyl-N-methyltrifluoroacetamide (MTBSTFA) with 1% tert-butyldimethylchlorosilane (tBDMCS) (Regis Technologies) at 45°C for 30 min. Polar derivatives were analyzed by GC-MS using a DB-35MS column (30m x 0.25mm i.d. x 0.25µm, Agilent J&W Scientific) installed in an Agilent 7890B gas chromatograph (GC) interfaced with an Agilent 5977A mass spectrometer (MS) with an XTR ion source. The dried lower chloroform phase was derivatized to form fatty acid methyl esters (FAMEs) via addition of 500µL 2% H_2SO_4 in MeOH and incubation at 50°C for 2h. FAMEs were extracted via addition of 100µL saturated salt solution and 2 500µL hexane washes. These were analyzed using a Select FAME column (100m × 0.25mm i.d.) installed in an Agilent 7890A GC interfaced with an Agilent 5975C MS using the following

temperature program: 80°C initial, increase by 20°C/min to 170°C, increase by 1°C/min to 204°C, then 20°C/min to 250°C and hold for 10 min. The percent isotopologue distribution of each fatty acid and polar metabolite was determined and corrected for natural abundance using in-house algorithms adapted from Fernandez et al. (*55*). Mole percent enrichment (MPE) was calculated via the following equation:

$$\frac{\sum_{i=1}^{n} M_i \cdot i}{n}$$

Isotopomer spectral analysis (ISA) of fatty acids

Mass isotopomer distributions were determined by integrating metabolite ion fragments and correcting for natural abundance using in-house algorithms as previously described (*10*). The ISA compares a measured fatty acid isotopomer distribution to one that is simulated using a reaction network for palmitate synthesis, whereby 8 AcCoA molecules are consumed to form one palmitate molecule. Models were also generated for OCFA synthesis, whereby 1 PropCoA and 6-7 AcCoA molecules are consumed to form one OCFA as previously described (*13*). Parameters for the relative enrichment of the lipogenic AcCoA pool from a given [^{13}C] tracer and the percentage of fatty acids that are *de novo* synthesized are extracted from a best-fit model using INCA v1.6 metabolic flux analysis software package (*38*). The 95% confidence intervals for both parameters were estimated by evaluating the sensitivity of the sum of squared residuals between measured and simulated fatty acid mass isotopomer distributions to small flux variations.

Metabolic Flux Analysis

^{13}C MFA was conducted using INCA, a software package based on elementary metabolite unit (EMU) framework (*38*, *56*). Fluxes through the metabolic network comprising of glycolysis, the pentose phosphate pathway, the TCA cycle, BCAA catabolism, and fatty acid synthesis and oxidation were estimated by minimizing the sum of squared residuals between experimental MIDs and extracellular fluxes using nonlinear least squares regression for differentiated 3T3-L1 adipocytes traced with [U-$^{13}C_6$]glucose, [U-$^{13}C_5$]valine, [U-$^{13}C_6$]leucine. The best global fit was found after estimating 20 times using random initial guesses for all fluxes in the metabolic network. A χ^2 statistical test was applied to assess the goodness-of-fit using α of 0.01. The 95% confidence intervals for each flux in the metabolic network were estimated by sensitivity analysis due to minor flux variations (*57*). See Supplementary Table 1 for metabolites used in the analysis, below for assumptions, and Supplementary Tables 2-3 for raw flux values.

^{13}C metabolic flux analysis was conducted under the following assumptions:

- Cells were assumed to be at metabolic and isotopic steady state, i.e. intracellular free metabolite pool size and ^{13}C enrichments are constant.
- Per well extracellular flux of glucose, lactate, glutamine, glutamate, alanine, valine, and leucine were assumed to be constant over the course of the labeling experiments.
- Experimental replicates from all three tracers were entered into INCA v2.0 and used simultaneously to estimate fluxes for sgControl and sgBckdha, resulting in tighter confidence intervals.
- Cells were assumed to be terminally differentiated and did not divert resources towards biomass synthesis.

- Succinate and fumarate are structurally symmetric and can be enzymatically converted to their subsequent products in either configuration.
- Labeled CO_2 release during decarboxylation reactions is diluted upon release and does not reincorporate during carboxylation reactions.
- Separate mitochondrial and cytosolic pools of aspartate, oxaloacetate, malate, fumarate, pyruvate, acetyl-CoA, glutamate, and glutamine were modeled with exchange fluxes for malate, aspartate, glutamate, and glutamine.
- Relative branching of glucose flux to the oxidative pentose phosphate pathway (PPP) relative to the glucose uptake flux was set to 0.3%. (*40*)

RNA isolation and quantitative RT-PCR analysis

Total RNA was purified from cultured cells using Trizol Reagent (Life Technologies) per the manufacturer's instructions. First-strand cDNA was synthesized from 0.5µg of total RNA using High-capacity cDNA Reverse Transcription Kit with RNase inhibitor (Applied Biosystems) according to the manufacturer's instructions. Individual 10µl SYBR Green real-time PCR reactions consisted of 2µL of diluted cDNA, 5µL of SYBR Green Supermix (Bio-Rad), and 1µL of primer master mix containing each forward and reverse primer at 5µM. For standardization of quantification, ribosomal RNA RPL27 was amplified simultaneously. The PCR was carried out on 96-well plates on a CFX Connect Real time System (Bio-Rad) using a three-stage program provided by the manufacturer: 95°C hot-start for 3 min, 40 cycles of 95°C for 10s and 60°C for 30s, followed by a 0.5°C/5 sec meltcurve generation protocol. Gene-specific primers used are listed in Supplementary Table 5.

RNA-seq library preparation

Cells were lysed in Trizol and total RNA was extracted per manufacturer's instructions. Stranded RNA-Seq libraries were prepared from polyA-enriched mRNA using the Illumina Stranded mRNA library prep kit. Library construction and sequencing was performed by the University of California San Diego (UCSD) Institute for Genomic Medicine. Libraries were run as PE100 on a NovaSeq S4 to a depth of ~25 million reads.

RNASeq Analysis and Gene Set Enrichment Analysis

The Kallisto/Sleuth differential expression pipeline analysis was performed for paired triplicate samples of NT, Bckdha, and Acad8 KO. The index was obtained from Pachter lab Kallisto website "Ensembl Transcriptomes v96", mus_musculus.tar.gz. Kallisto was run for paired-end read quantification with sequence based bias correction (--bias) and 100 bootstraps (*58*). Normalized transcript abundances were further passed into sleuth using R, which were then aggregated to gene level (*59*). Ultimately, a pairwise Wald test was performed to compare sgControl v. sgBckdha and sgControl v. sgAcad8 using sleuth.

GSEA analysis using the KEGG pathway functional database was performed using WEB-based GEne SeT AnaLysis Toolkit (WebGestalt). A rank score was calculated through multiplication of the q-value with the sign of the fold change of sgBckdha and sgControl adipocytes. Only significantly differentially expressed genes ($q<0.05$) were included in the analysis. Redundancy reduction of the enriched gene sets was set to "All." The MSigDB Hallmarks pathway functional database was downloaded in gene symbol format (http://www.gsea-msigdb.org/gsea/msigdb/collections.jsp) (*60, 61*). As this is a human pathway database, the

differentially expressed genes in the present study were first mapped to their human homologs using the publicly available mouse human genome homology database compiled by the mouse genome informatics organization (http://www.informatics.jax.org/downloads/reports/) (*62*). GSEA analysis was then conducted using the WebGestalt platform, using the hallmarks pathway set as a custom database, and the human homologs of the differentially expressed genes ($q<0.05$) in this study and their associated rank score as the input gene list.

Respirometry

Respirometry was conducted using a Seahorse XF96E Analyzer. For respiration studies, cells were plated at 5,000 cells/well and maintained in 2μg/mL puromycin-containing media until confluence was reached and differentiation was performed as described above. 8 days after differentiation was initiated, growth medium was replaced with DMEM (Sigma #5030) supplemented with 25mM HEPES, 8mM glucose, 2mM glutamine, and 1 mM pyruvate. Mitochondrial respiration is calculated as the oxygen consumption rate sensitive to 1μM rotenone and 2μM antimycin A. Maximal respiration was calculated as the difference between the maximum respiratory rate in response to 5μM FCCP that was sensitive to antimycin A. Immediately after the experiment, cells were gently washed with PBS and either a) fixed with 4% paraformaldehyde and stained with CyQuant (Life Technologies) to determine cell number for normalization purposes or b) solubilized in RIPA buffer and quantified using BCA assay. Data from n=3 independent experiments is depicted after normalization within each experiment.

Animal study

Animal handling and care followed the NIH Guide for Care and Use of Laboratory Animals. The experimental protocol was approved by the Institutional Animal Care and Use Committee. 5 week old male C57BL/6J mice were obtained from Jackson Laboratories and *ad lib* fed a custom 20% kcal fat diet (TD. 160091) for 15 weeks from 6 weeks of age. Diets and incorporated isotopes were obtained from Envigo Teklad Diets and Cambridge isotopes respectively. For the final 3 weeks, 25% of the total valine and leucine in the diet was replaced with [U-$^{13}C_5$-^{15}N]valine and [U-$^{13}C_6$-^{15}N]leucine so that there was 3 g [U-$^{13}C_5$-^{15}N]valine /100 grams protein and 4 g [U-$^{13}C_6$-^{15}N]leucine/100 grams protein in both diets. Mice were fasted overnight prior to plasma and tissue collection and samples were immediately snap frozen in liquid N_2.

Statistical analyses

All experiments were repeated at least 3 times and data from 1 representative experiment is shown. For analyses involving 2 groups, a two-tailed Student's t-test was performed. For analyses with 3 groups or more, a one- or two-way ANOVA was performed as appropriate. Dunnett correction for multiple comparisons was performed for all analyses except Seahorse measurements.

Figure Legends

Figure 1. *Bckdha* deficiency alters systemic amino acid metabolism

A. Western blot of BCKDHA and β-ACTIN
B. Brightfield images of differentiated Control and sgBckdha adipocytes 7 days post-induction of differentiation (scale bar = 400μm)

C. Mole percent enrichment of citrate from [U-$^{13}C_6$]leucine in sgControl and sgBckdha adipocytes.

D. Expression of adipocyte differentiation markers normalized to sgControl

E. Heat map of the fold change of the abundance of intracellular amino acids in *Bckdha*-deficient adipocytes normalized to sgControl

F. Normalized relative uptake of leucine, isoleucine, and valine in Control and *Bckdha*-deficient adipocytes

Data are presented as means ± SEM (C, F) or means ± SD (D) with three cellular replicates. One-way ANOVA (C) or two-way ANOVA (D, F) all with Dunnett's correction for multiple comparisons. Significance in all is compared to sgControl. Results are depicted from one representative experiment which was repeated independently at least three times. *p<0.05, **p<0.01, ***p<0.001.

Figure 2. *Bckdha* deficiency broadly alters gene expression

A. Volcano plots of differentially expressed genes in *Bckdha*-deficient adipocytes compared to Control adipocytes

B. Gene set enrichment analysis of *Bckdha*-deficient adipocytes generated using WEB-based GEne SeT AnaLysis Toolkit (WebGestalt)

Figure 3: Glucose metabolism is reprogrammed in *Bckdha*-deficient adipocytes

A. Simplified metabolic map of central carbon metabolism

B. Molar amount of glucose uptake in Control or *Bckdha*-deficient adipocytes over 48 hours

C. Molar amount of lactate secretion in Control or *Bckdha*-deficient adipocytes over 48 hours

D. Ratio of lactate secretion to glucose uptake after 48 hours

E. Intracellular lactate to pyruvate ratio

Data are presented as means ± SD (B-E) with three cellular replicates. One-way ANOVA with Dunnett's correction for multiple comparisons (B-E). Significance in all is compared to sgControl. Results are depicted from one representative experiment which was repeated independently at least three times.

*p<0.05, **p<0.01, ***p<0.001.

Figure 4: Respiration is negatively impacted by Bckdha deficiency

A. Relative abundance of TCA cycle intermediates in *Bckdha*-deficient adipocytes normalized to sgControl adipocytes

B. Normalized oxygen consumption rate of 3T3-L1 Control or *Bckdha*-deficient adipocytes treated with the indicated pharmacological inhibitors (n=3 experiments internally normalized to sgControl)

C. Mole percent enrichment (MPE) of TCA cycle intermediates after 48 hours of incubation with [U-$^{13}C_6$]glucose

D. MPE of TCA cycle intermediates after 48 hours of incubation with [U-$^{13}C_5$]glutamine

E. Normalized MPE from dual [U-$^{13}C_6$]leucine and [U-$^{13}C_5$]valine tracing in cultured 3T3-L1 adipocytes and mice epididymal white adipose tissue (eWAT) after 21 days of labeled chow feeding

Data are presented as means ± SEM with six cellular replicates (B), means ± SD with three cellular replicates (C-D), or means ± SEM with seven tissue replicates and three cellular replicates (E). Two-way ANOVA with Dunnett's correction for multiple comparisons (A-D). Significance in all is compared to sgControl. Results are depicted from one representative experiment which was repeated independently at least three times.

*p<0.05, **p<0.01, ***p<0.001.

Figure 5: Altering BCAA catabolism alters fatty acid diversity

A. Relative fold change in total odd- and even- straight-chain fatty acids in *Bckdha*-deficient 3T3-L1 adipocytes normalized to Control adipocytes.
B. Relative fold change in total branched-chain fatty acids (BCFAs) in *Bckdha*-deficient 3T3-L1 adipocytes normalized to Control adipocytes.
C. Contribution of [U-$^{13}C_6$]glucose to the lipogenic AcCoA pool used for *de novo* lipogenesis (DNL)
D. Percent of fatty acids derived from *de novo* lipogenesis in Control and *Bckdha*-deficient 3T3-L1 adipocytes over 48 hours obtained via isotopomer spectral analysis (ISA).
E. Molar amount of indicated fatty acids synthesized over 48 hours obtained by combining individual FA DNL values with pool size
F. Desaturation index in Control and *Bckdha*-deficient 3T3-L1 adipocytes

Data are presented as means ± SD (A, B, F), means ± 95% C.I. (C-D), and means ± SEM (E) with three cellular replicates. Two-way ANOVA (A-B, F) or one-way ANOVA of the total values (E) all with Dunnett's correction for multiple comparisons and non-overlapping 95% C.I.

(C, D). Significance in all is compared to sgControl. Results are depicted from one representative experiment which was repeated independently at least three times.

*p<0.05, **p<0.01, ***p<0.001.

Figure 6. Metabolic flux analysis reveals significant reprogramming of glycolysis and TCA metabolism

A. Map of core MFA model. Values are presented as net flux (exchange flux). Blue text is sgControl, red text is sgBckdha. Blue arrows indicate a flux is decreased in sgBckdha compared to sgControl, while a red arrow indicates an increase in flux in sgBckdha. Bold text indicates significantly different reactions.

Figure 7. *Acad8* deficiency impacts anaplerosis and alters OCFA and BCFA accumulation

A. Western blot of ACAD8 and β-ACTIN
B. Brightfield images of differentiated Control and sgAcad8 adipocytes 7 days post-induction of differentiation (scale bar = 400μm)
C. Volcano plots of differentially expressed genes in *Acad8*-deficient adipocytes compared to Control adipocytes
D. Heat map of the fold change of the abundance of intracellular TCA cycle intermediates in *Bckdha*-deficient adipocytes normalized to sgControl
E. Citrate mass isotopomer distribution (MID) after 48 hours of incubation with [U-$^{13}C_6$]glucose
F. Relative fold change in total odd- and even- straight-chain fatty acids in *Acad8*-deficient 3T3-L1 adipocytes normalized to Control adipocytes.

G. Relative fold change in total branched-chain fatty acids (BCFAs) in *Acad8*-deficient 3T3-L1 adipocytes normalized to Control adipocytes.

Data are presented as means ± SD (E-G) with three cellular replicates. Two-way ANOVA (E-G). Significance in all is compared to sgControl. Results are depicted from one representative experiment which was repeated independently at least three times.

*p<0.05, **p<0.01, ***p<0.001.

Supplementary Figures

Supplementary Figure 1. *Bckdha* deficiency alters BCKA levels and amino acid metabolism

A. Ratio of α-ketoisocaproate (KIC) to leucine in Control and *Bckdha*-deficient adipocytes
B. Normalized relative uptake or efflux of amino acids in Control and *Bckdha*-deficient adipocytes
C. Mole percent enrichment (MPE) of non-essential amino acids alanine, glycine, serine, proline, aspartate, and glutamine from [U-$^{13}C_6$]glucose

Data are presented as means ± SD (A-C) with three cellular replicates. One-way ANOVA (A) or two-way ANOVA (B-C). Significance in all is compared to sgControl. Results are depicted from one representative experiment which was repeated independently at least three times.

*p<0.05, **p<0.01, ***p<0.001.

Supplementary Figure 2. Bckdha deficiency alters transcription and glucose metabolism without affecting mitochondrial number:

A. Gene set enrichment analysis of *Bckdha*-deficient adipocytes generated using WEB-based GEne SeT AnaLysis Toolkit (WebGestalt) using the MsigDB biological processes hallmarks database
B. Citrate mass isotopomer distribution (MID) after 48 hours of incubation with [U-$^{13}C_6$]glucose
C. Normalized gene expression of mitochondrial DNA markers in Control and *Bckdha*-deficient adipocytes

Data are presented as means ± SD (B, C) with three cellular replicates. Two-way ANOVA (B, C). Significance in all is compared to sgControl. Results are depicted from one representative experiment which was repeated independently at least three times.

*$p<0.05$, **$p<0.01$, ***$p<0.001$.

References:

1. M. D. Neinast *et al.*, Quantitative Analysis of the Whole-Body Metabolic Fate of Branched-Chain Amino Acids. *Cell Metab* **29**, 417-429.e414 (2019).
2. P. Nicklin *et al.*, Bidirectional transport of amino acids regulates mTOR and autophagy. *Cell* **136**, 521-534 (2009).
3. H. A. Zimmerman, K. C. Olson, G. Chen, C. J. Lynch, Adipose transplant for inborn errors of branched chain amino acid metabolism in mice. *Molecular genetics and metabolism* **109**, 345-353 (2013).
4. M. A. Herman, P. She, O. D. Peroni, C. J. Lynch, B. B. Kahn, Adipose tissue branched chain amino acid (BCAA) metabolism modulates circulating BCAA levels. *The Journal of biological chemistry* **285**, 11348-11356 (2010).
5. T. Yoneshiro *et al.*, BCAA catabolism in brown fat controls energy homeostasis through SLC25A44. *Nature* **572**, 614-619 (2019).
6. E. Zaganjor *et al.*, SIRT4 is an early regulator of branched-chain amino acid catabolism that promotes adipogenesis. *Cell reports* **36**, 109345 (2021).
7. A. Halama *et al.*, Metabolic switch during adipogenesis: From branched chain amino acid catabolism to lipid synthesis. *Arch Biochem Biophys* **589**, 93-107 (2016).
8. D. T. Chuang, C. W. Hu, M. S. Patel, Induction of the branched-chain 2-oxo acid dehydrogenase complex in 3T3-L1 adipocytes during differentiation. *The Biochemical journal* **214**, 177-181 (1983).
9. S. B. Crown, N. Marze, M. R. Antoniewicz, Catabolism of Branched Chain Amino Acids Contributes Significantly to Synthesis of Odd-Chain and Even-Chain Fatty Acids in 3T3-L1 Adipocytes. *PLOS ONE* **10**, (2015).
10. C. R. Green *et al.*, Branched-chain amino acid catabolism fuels adipocyte differentiation and lipogenesis. *Nature chemical biology* **12**, 15-21 (2016).
11. N. Y. Kedishvili, K. M. Popov, J. A. Jaskiewicz, R. A. Harris, Coordinated expression of valine catabolic enzymes during adipogenesis: analysis of activity, mRNA, protein levels, and metabolic consequences. *Archives of biochemistry and biophysics* **315**, 317-322 (1994).
12. D. E. Lackey *et al.*, Regulation of adipose branched-chain amino acid catabolism enzyme expression and cross-adipose amino acid flux in human obesity. *American journal of physiology. Endocrinology and metabolism* **304**, 87 (2013).
13. M. Wallace *et al.*, Enzyme promiscuity drives branched-chain fatty acid synthesis in adipose tissues. *Nature Chemical Biology* **14**, 1021 (2018).
14. C. Jang *et al.*, A branched-chain amino acid metabolite drives vascular fatty acid transport and causes insulin resistance. *Nat Med* **22**, 421-426 (2016).
15. Q. X. Ma *et al.*, BCAA-BCKA axis regulates WAT browning through acetylation of PRDM16. *Nat Metab* **4**, 106-122 (2022).
16. S. Trefely *et al.*, Quantitative subcellular acyl-CoA analysis reveals distinct nuclear metabolism and isoleucine-dependent histone propionylation. *Mol Cell* **82**, 447-462.e446 (2022).
17. C. B. Newgard *et al.*, A branched-chain amino acid-related metabolic signature that differentiates obese and lean humans and contributes to insulin resistance. *Cell metabolism* **9**, 311-326 (2009).
18. T. J. Wang *et al.*, Metabolite profiles and the risk of developing diabetes. *Nature medicine* **17**, 448-453 (2011).
19. M. Guasch-Ferré *et al.*, Metabolomics in Prediabetes and Diabetes: A Systematic Review and Meta-analysis. *Diabetes Care* **39**, 833-846 (2016).
20. M. M. Boulet *et al.*, Alterations of plasma metabolite profiles related to adipose tissue distribution and cardiometabolic risk. *Am J Physiol Endocrinol Metab* **309**, E736-746 (2015).
21. V. Cifarelli *et al.*, Decreased adipose tissue oxygenation associates with insulin resistance in individuals with obesity. *J Clin Invest* **130**, 6688-6699 (2020).
22. W. Sun, S. Modica, H. Dong, C. Wolfrum, Plasticity and heterogeneity of thermogenic adipose tissue. *Nat Metab* **3**, 751-761 (2021).

23. A. Sakers, M. K. De Siqueira, P. Seale, C. J. Villanueva, Adipose-tissue plasticity in health and disease. *Cell* **185**, 419-446 (2022).
24. K. L. Spalding *et al.*, Dynamics of fat cell turnover in humans. *Nature* **453**, 783-787 (2008).
25. M. S. Nilsen *et al.*, 3-Hydroxyisobutyrate, A Strong Marker of Insulin Resistance in Type 2 Diabetes and Obesity That Modulates White and Brown Adipocyte Metabolism. *Diabetes* **69**, 1903-1916 (2020).
26. T. Yoneshiro *et al.*, Metabolic flexibility via mitochondrial BCAA carrier SLC25A44 is required for optimal fever. *Elife* **10**, (2021).
27. L. C. Burrage, S. C. S. Nagamani, P. M. Campeau, B. H. Lee, Branched-chain amino acid metabolism: from rare Mendelian diseases to more common disorders. *Human Molecular Genetics* **23**, R1-8 (2014).
28. I. Knerr, N. Weinhold, J. Vockley, K. M. Gibson, Advances and challenges in the treatment of branched-chain amino/keto acid metabolic defects. *J Inherit Metab Dis* **35**, 29-40 (2012).
29. K. A. Strauss, D. H. Morton, Branched-chain Ketoacyl Dehydrogenase Deficiency: Maple Syrup Disease. *Current treatment options in neurology* **5**, 329-341 (2003).
30. S. Schönberger, B. Schweiger, B. Schwahn, M. Schwarz, U. Wendel, Dysmyelination in the brain of adolescents and young adults with maple syrup urine disease. *Molecular Genetics and Metabolism* **82**, 69-75 (2004).
31. J. Korein, C. Sansaricq, M. Kalmijn, J. Honig, B. Lange, Maple syrup urine disease: clinical, EEG, and plasma amino acid correlations with a theoretical mechanism of acute neurotoxicity. *Int J Neurosci* **79**, 21-45 (1994).
32. D. H. Morton, K. A. Strauss, D. L. Robinson, E. G. Puffenberger, R. I. Kelley, Diagnosis and treatment of maple syrup disease: a study of 36 patients. *Pediatrics* **109**, 999-1008 (2002).
33. J. Y. Lee *et al.*, Maple syrup urine disease (MSUD)--clinical profile of 47 Filipino patients. *J Inherit Metab Dis* **31 Suppl 2**, S281-285 (2008).
34. T. V. Nguyen *et al.*, Identification of isobutyryl-CoA dehydrogenase and its deficiency in humans. *Mol Genet Metab* **77**, 68-79 (2002).
35. J. W. Yun *et al.*, A novel ACAD8 mutation in asymptomatic patients with isobutyryl-CoA dehydrogenase deficiency and a review of the ACAD8 mutation spectrum. *Clin Genet* **87**, 196-198 (2015).
36. S. Santra, A. Macdonald, M. A. Preece, R. K. Olsen, B. S. Andresen, Long-term outcome of isobutyryl-CoA dehydrogenase deficiency diagnosed following an episode of ketotic hypoglycaemia. *Molecular Genetics and Metabolism Reports* **10**, 28-30 (2017).
37. M. Liu *et al.*, Mechanism of SEMA3G knockdown-mediated attenuation of high-fat diet-induced obesity. *J Endocrinol* **244**, 223-236 (2020).
38. J. D. Young, INCA: a computational platform for isotopically non-stationary metabolic flux analysis. *Bioinformatics* **30**, 1333-1335 (2014).
39. M. M. Islam *et al.*, A novel branched-chain amino acid metabolon. Protein-protein interactions in a supramolecular complex. *J Biol Chem* **282**, 11893-11903 (2007).
40. L. Liu *et al.*, Malic enzyme tracers reveal hypoxia-induced switch in adipocyte NADPH pathway usage. *Nature chemical biology* **12**, 345-352 (2016).
41. E. H. Oates, M. R. Antoniewicz, Coordinated reprogramming of metabolism and cell function in adipocytes from proliferation to differentiation. *Metab Eng* **69**, 221-230 (2022).
42. M. Zhou *et al.*, Targeting BCAA Catabolism to Treat Obesity-Associated Insulin Resistance. *Diabetes* **68**, 1730-1746 (2019).
43. J. Wang *et al.*, BCAA Catabolic Defect Alters Glucose Metabolism in Lean Mice. *Front Physiol* **10**, 1140 (2019).
44. D. Biswas *et al.*, Branched-chain ketoacid overload inhibits insulin action in the muscle. *J Biol Chem* **295**, 15597-15621 (2020).
45. H. Sun *et al.*, Catabolic Defect of Branched-Chain Amino Acids Promotes Heart Failure. *Circulation* **133**, 2038-2049 (2016).

46. Y. Kishimoto, M. Williams, H. W. Moser, C. Hignite, K. Biermann, Branched-chain and odd-numbered fatty acids and aldehydes in the nervous system of a patient with deranged vitamin B 12 metabolism. *Journal of lipid research* **14**, 69-77 (1973).
47. X. Su *et al.*, Adipose tissue monomethyl branched-chain fatty acids and insulin sensitivity: Effects of obesity and weight loss. *Obesity* **23**, 329-334 (2014).
48. A. Mika *et al.*, A comprehensive study of serum odd- and branched-chain fatty acids in patients with excess weight. *Obesity* **24**, 1669-1676 (2016).
49. M. C. Sawh *et al.*, Dairy Fat Intake, Plasma Pentadecanoic Acid, and Plasma Iso-heptadecanoic Acid Are Inversely Associated With Liver Fat in Children. *J Pediatr Gastroenterol Nutr* **72**, e90-e96 (2021).
50. R. Mercier, P. Domínguez-Cuevas, J. Errington, Crucial Role for Membrane Fluidity in Proliferation of Primitive Cells. *Cell Reports* **1**, 417-423 (2012).
51. I. Budin *et al.*, Viscous control of cellular respiration by membrane lipid composition. *Science* **362**, 1186-1189 (2018).
52. L. Liu *et al.*, Human fetal intestinal epithelial cells metabolize and incorporate branched chain fatty acids in a structure specific manner. *Prostaglandins Leukot Essent Fatty Acids* **116**, 32-39 (2017).
53. N. E. Sanjana, O. Shalem, F. Zhang, Improved vectors and genome-wide libraries for CRISPR screening. *Nature Methods* **11**, 783-784 (2014).
54. T. Cordes, C. M. Metallo, in *High-Throughput Metabolomics: Methods and Protocols*, A. D'Alessandro, Ed. (Springer New York, New York, NY, 2019), pp. 219-241.
55. C. A. Fernandez, C. Des Rosiers, S. F. Previs, F. David, H. Brunengraber, Correction of 13C mass isotopomer distributions for natural stable isotope abundance. *J Mass Spectrom* **31**, 255-262 (1996).
56. J. D. Young, J. L. Walther, M. R. Antoniewicz, H. Yoo, G. Stephanopoulos, An elementary metabolite unit (EMU) based method of isotopically nonstationary flux analysis. *Biotechnol Bioeng* **99**, 686-699 (2008).
57. M. R. Antoniewicz, J. K. Kelleher, G. Stephanopoulos, Determination of confidence intervals of metabolic fluxes estimated from stable isotope measurements. *Metab Eng* **8**, 324-337 (2006).
58. N. L. Bray, H. Pimentel, P. Melsted, L. Pachter, Near-optimal probabilistic RNA-seq quantification. *Nat Biotechnol* **34**, 525-527 (2016).
59. H. Pimentel, N. L. Bray, S. Puente, P. Melsted, L. Pachter, Differential analysis of RNA-seq incorporating quantification uncertainty. *Nat Methods* **14**, 687-690 (2017).
60. A. Subramanian *et al.*, Gene set enrichment analysis: a knowledge-based approach for interpreting genome-wide expression profiles. *Proc Natl Acad Sci U S A* **102**, 15545-15550 (2005).
61. V. K. Mootha *et al.*, PGC-1alpha-responsive genes involved in oxidative phosphorylation are coordinately downregulated in human diabetes. *Nat Genet* **34**, 267-273 (2003).
62. C. J. Bult *et al.*, Mouse Genome Database (MGD) 2019. *Nucleic Acids Res* **47**, D801-D806 (2019).

Figure 1
Bckdha deficiency alters systemic amino acid metabolism

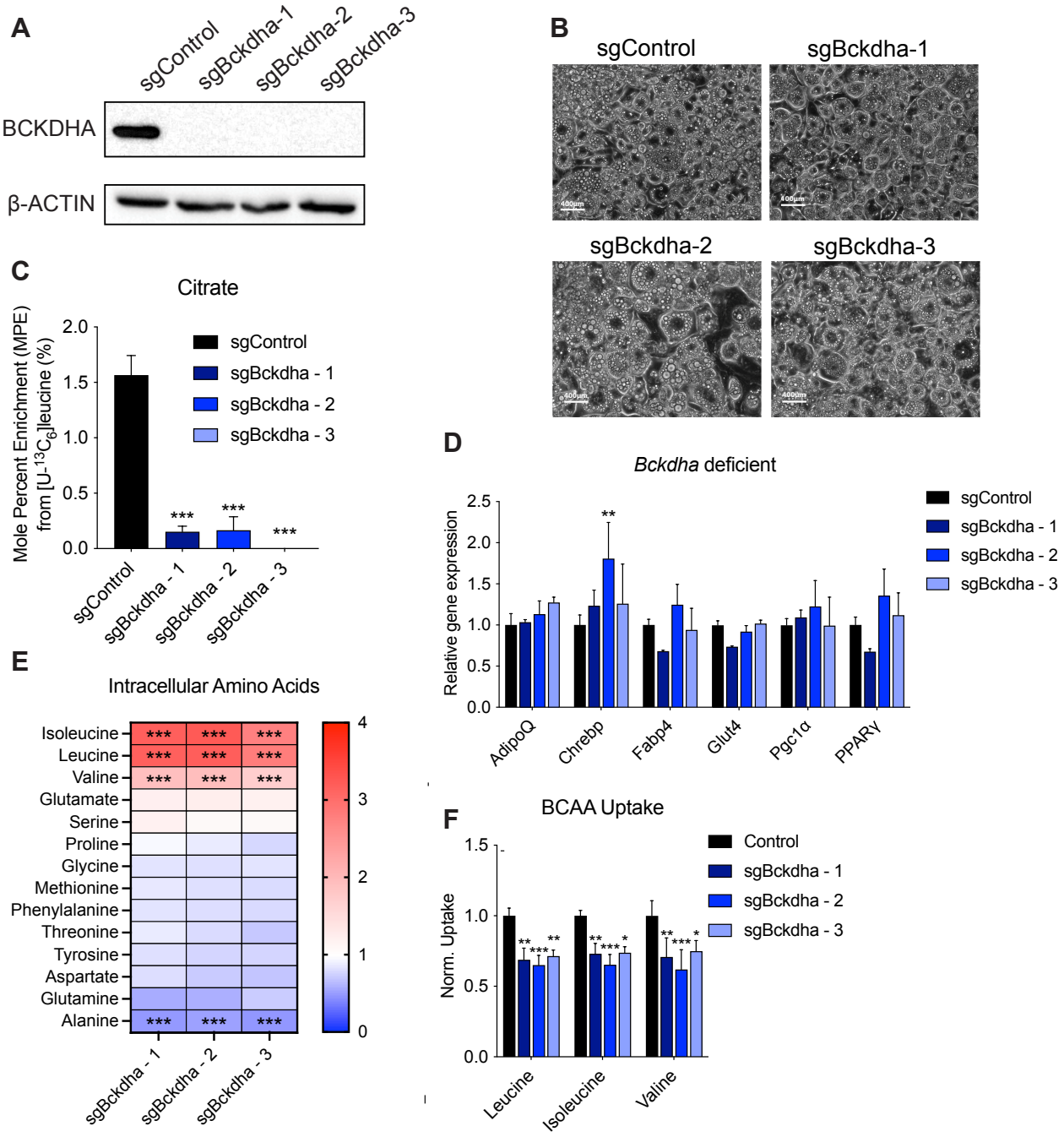

A. Western blot of Bckdha and Actin
B. Brightfield images of differentiated Control and sgBckdha adipocytes 7 days post-induction of differentiation (scale bar = 400μm)
C. Mole percent enrichment of citrate from [U-13C6]leucine in sgControl and sgBckdha adipocytes.
D. Expression of adipocyte differentiation markers normalized to sgControl
E. Heat map of the fold change of the abundance of intracellular amino acids in Bckdha-*deficient* adipocytes normalized to sgControl
F. Normalized relative uptake of leucine, isoleucine, and valine in Control and Bckdha-*deficient* adipocytes

Data are presented as means ± SEM (C, F) or means ± SD (D) with three cellular replicates. One-way ANOVA (C) or two-way ANOVA (D-F) all with Dunnett's correction for multiple comparisons. Significance in all is compared to sgControl. Results are depicted from one representative experiment which was repeated independently at least three times. *p<0.05, **p<0.01, ***p<0.001.

Figure 2
Bckdha deficiency broadly alters gene expression

A

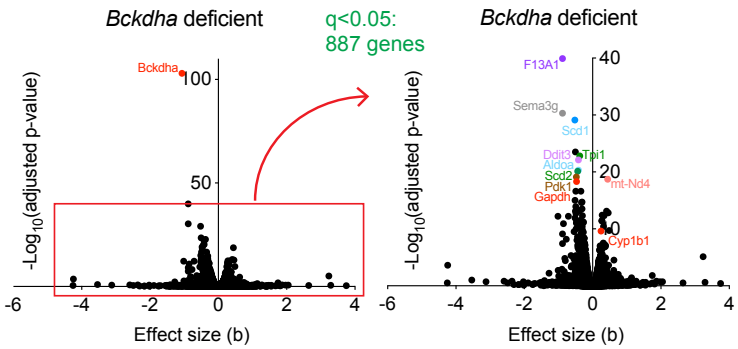

B

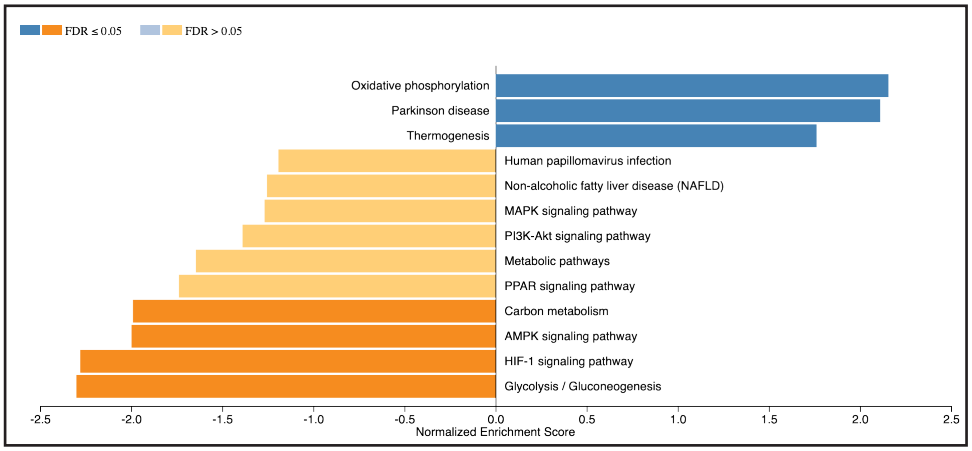

A. Volcano plots of differentially expressed genes in Bckdha-deficient adipocytes compared to Control adipocytes
B. Gene set enrichment analysis of Bckdha deficient adipocytes generated using WEB-based GEne SeT AnaLysis Toolkit (WebGestalt)

Figure 3
Glucose metabolism is reprogrammed in Bckdha deficient adipocytes

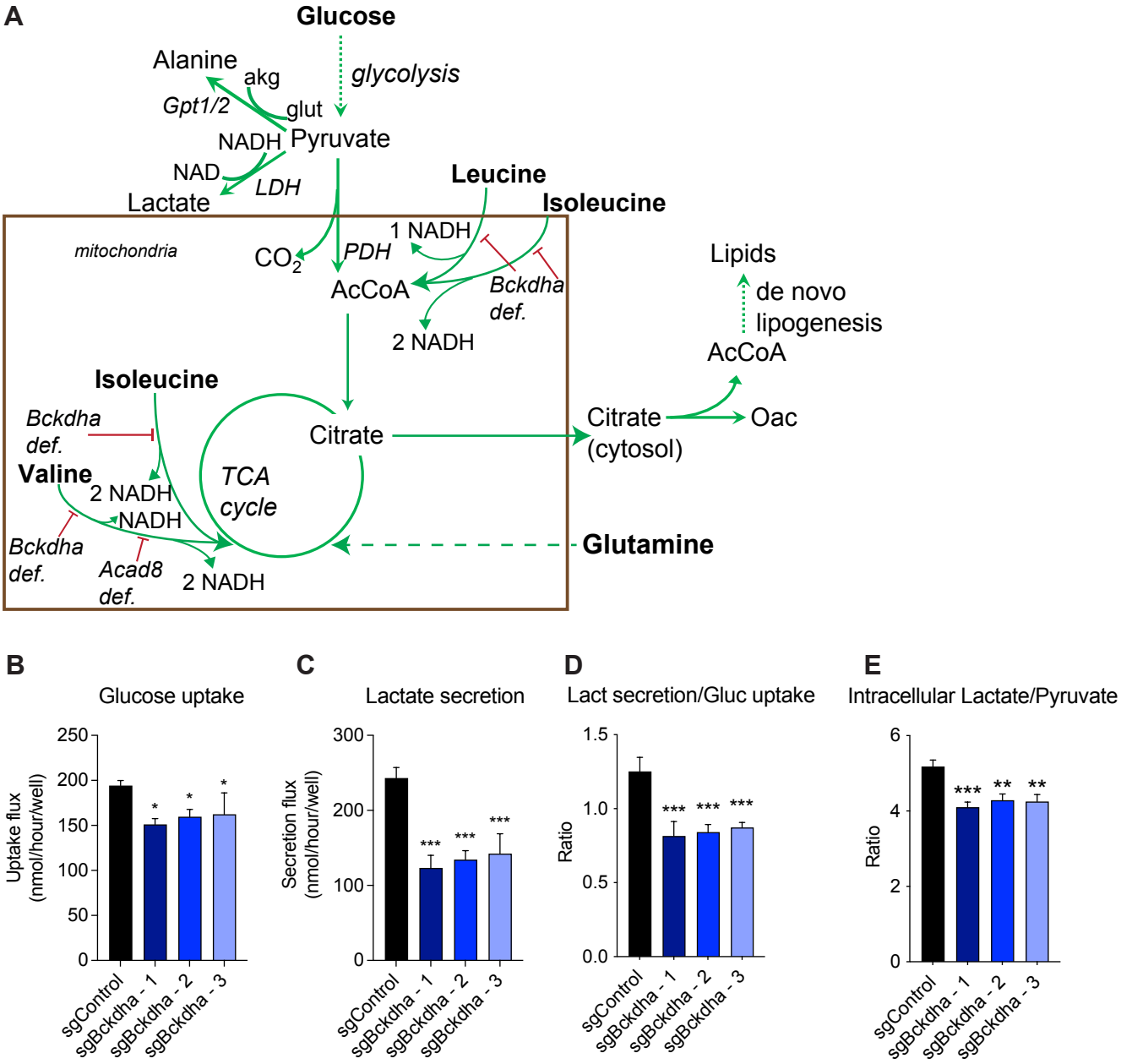

A. Simplified metabolic map of central carbon metabolism
B. Molar amount of glucose uptake in Control or Bckdha-deficient adipocytes over 48 hours
C. Molar amount of lactate secretion in Control or Bckdha-deficient adipocytes over 48 hours
C. Ratio of lactate secretion to glucose uptake after 48 hours
D. Intracellular lactate to pyruvate ratio

Data are presented as means ± SD (B-E) with three cellular replicates. One-way ANOVA with Dunnett's correction for multiple comparisons (B-E). Significance in all is compared to sgControl.
Results are depicted from one representative experiment which was repeated independently at least three times.
*p<0.05, **p<0.01, ***p<0.001.

Figure 4
Respiration is negatively impacted by Bckdha deficiency

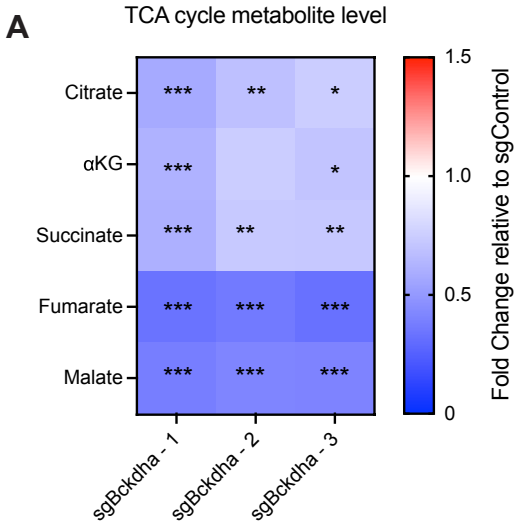

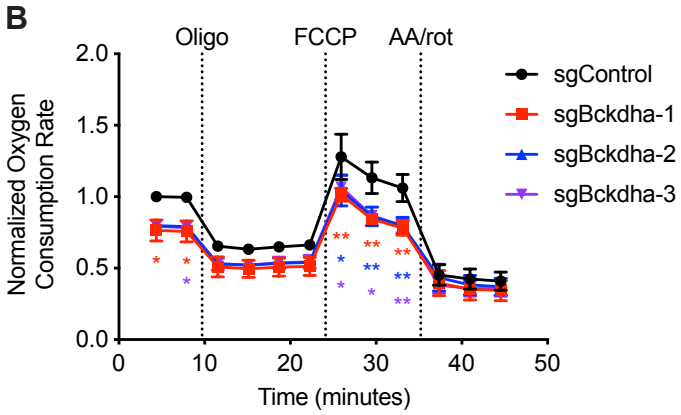

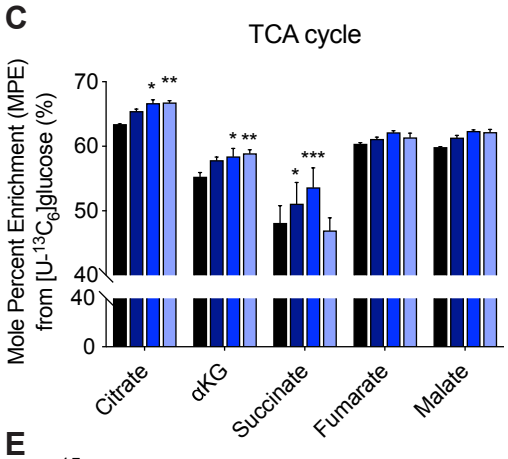

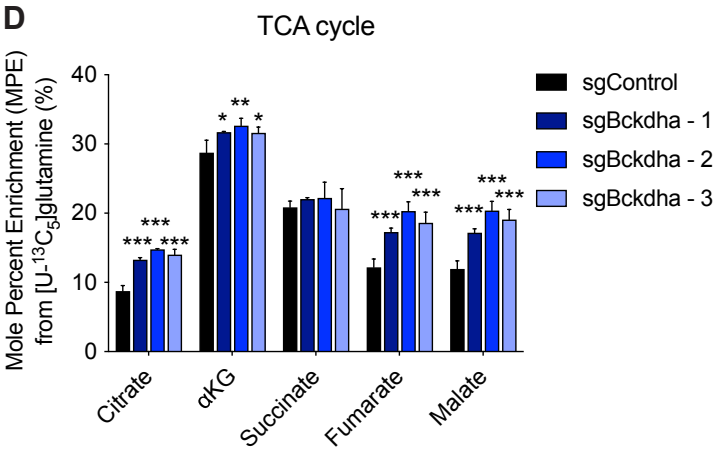

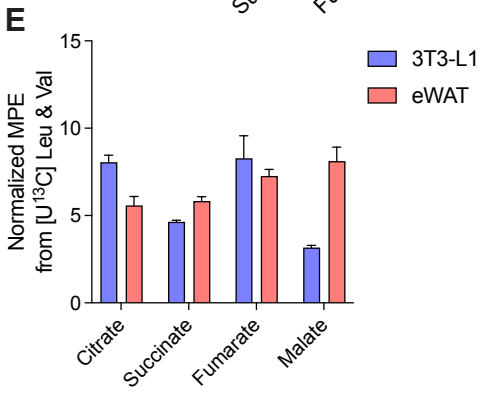

A. Relative abundance of TCA cycle intermediates in Bckdha-deficient adipocytes normalized to sgControl adipocytes
B. Normalized oxygen consumption rate of 3T3-L1 Control or Bckdha deficient adipocytes treated with the indicated pharmacological inhibitors (n=3 experiments internally normalized to sgControl)
C. Mole percent enrichment (MPE) of TCA cycle intermediates after 48 hours of incubation with [U-13C6]glucose
D. MPE of TCA cycle intermediates after 48 hours of incubation with [U-13C5]glutamine
E. Normalized MPE from dual [U-13C6]leucine and [U-13C5]valine tracing in cultured 3T3-L1 adipocytes and mice epididymal white adipose tissue (eWAT) after 21 days of labeled chow feeding

Data are presented as means ± SEM with six cellular replicates (B), means ± SD with three cellular replicates (C-D), or means ± SEM with seven tissue replicates and three cellular replicates (E). Significance in all is compared to sgControl. Results are depicted from one representative experiment which was repeated independently at least three times. *p<0.05, **p<0.01, ***p<0.001.

Figure 5
Altering BCAA catabolism alters fatty acid diversity

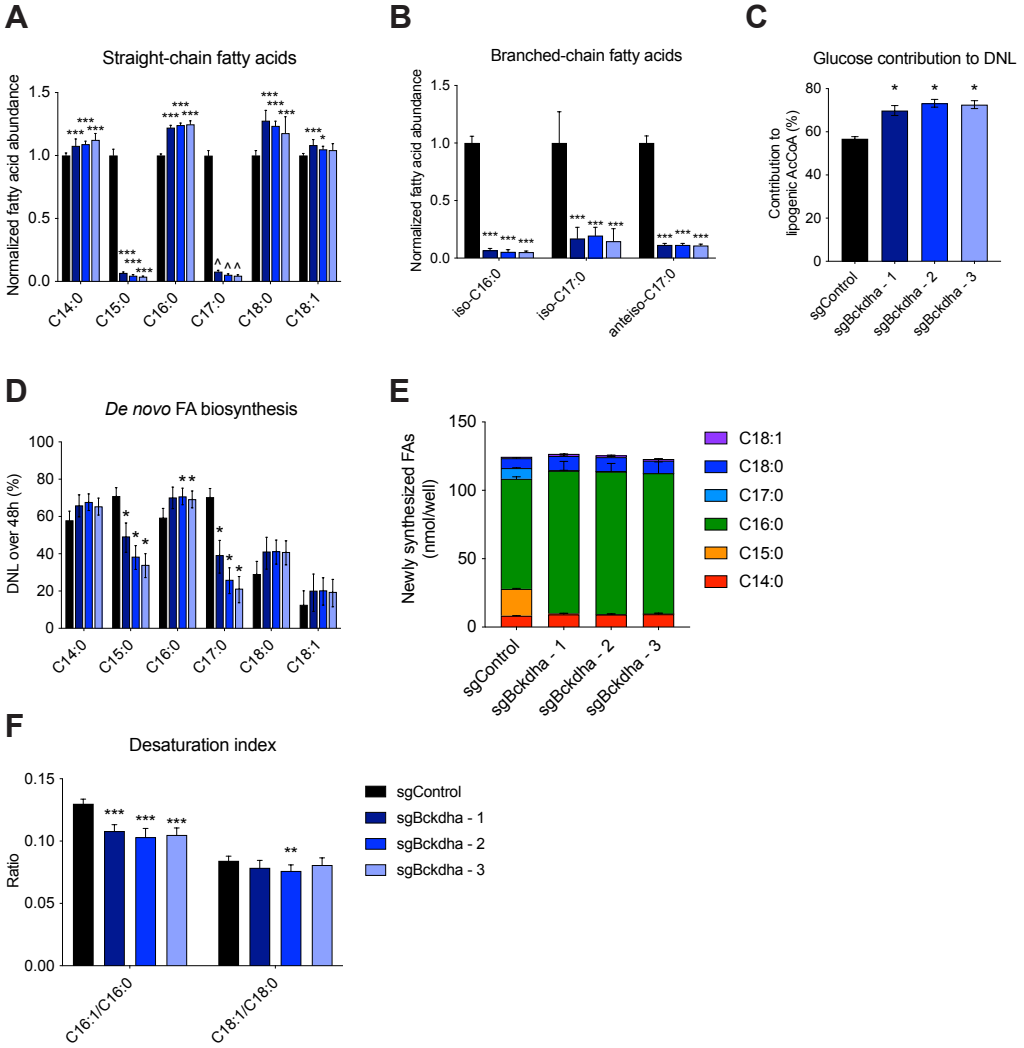

A. Relative fold change in total odd- and even- straight-chain fatty acids in Bckdha deficient 3T3-L1 adipocytes normalized to Control adipocytes.
B. Relative fold change in total branched-chain fatty acids (BCFAs) in Bckdha deficient 3T3-L1 adipocytes normalized to Control adipocytes.
C. Contribution of [U-13C6]glucose to the lipogenic AcCoA pool used for de novo lipogenesis (DNL)
D. Percent of fatty acids derived from de novo lipogenesis in Control and Bckdha deficient 3T3-L1 adipocytes over 48 hours obtained via isotopomer spectral analysis (ISA).
E. Molar amount of indicated fatty acids synthesized over 48 hours obtained by combining individual FA DNL values with pool size.
F. Desaturation index in Control and Bckdha deficient 3T3-L1 adipocytes.

Data are presented as means ± SD (A, B, F), means ± 95% C.I. (C-D), or means ± SEM (E) with three cellular replicates. Two-way ANOVA (A-B, F) or one-way ANOVA of the total values (E) all with Dunnett's correction for multiple comparisons and non-overlapping 95% C.I. (C, D). Significance in all is compared to sgControl. Results are depicted from one representative experiment which was repeated independently at least three times.
*p<0.05, **p<0.01, ***p<0.001.

Figure 6

Metabolic flux analysis reveals significant reprogramming of glycolysis and TCA metabolism

A

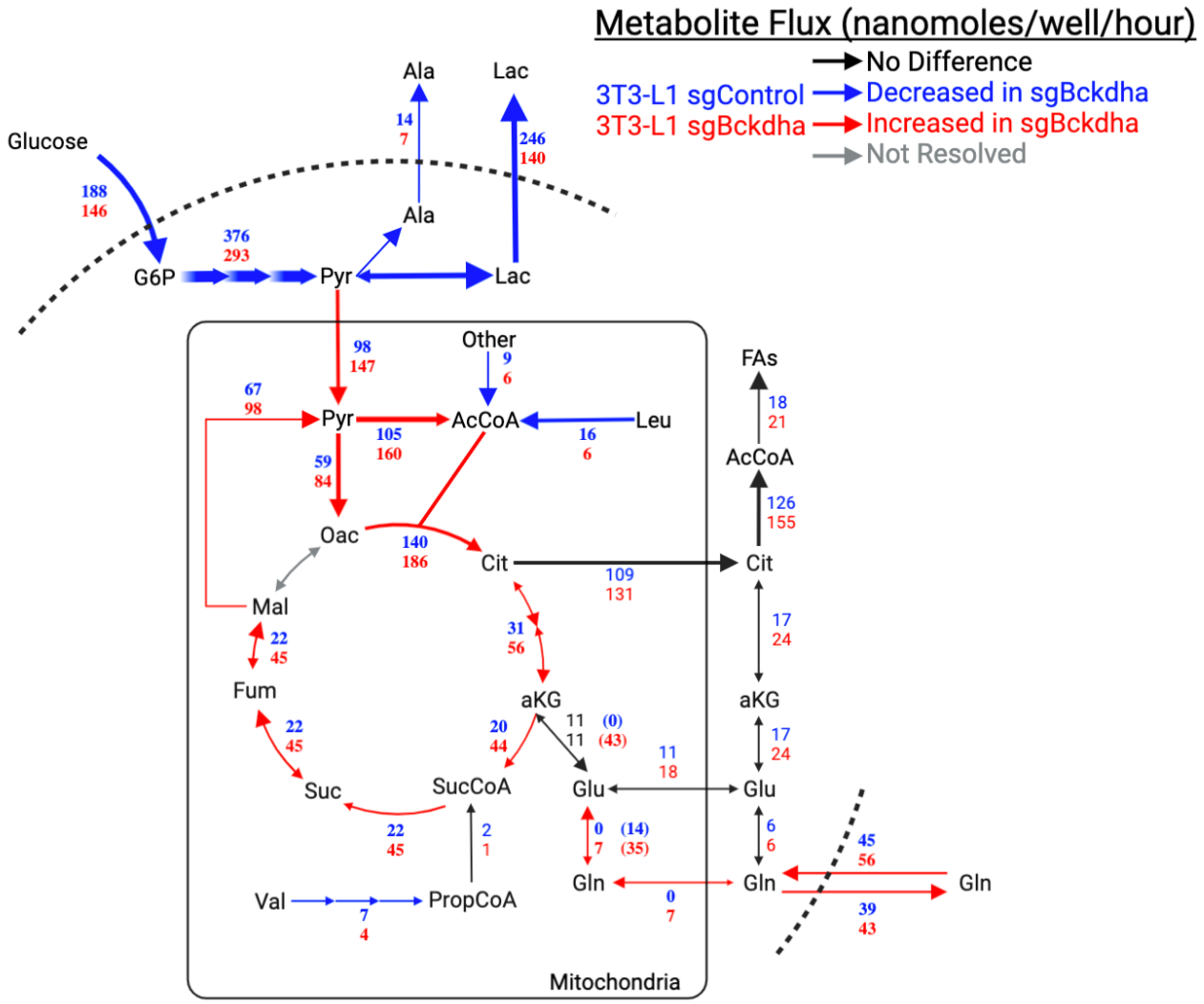

A. Map of core MFA model. Values are presented as flux (exchange flux). Blue text is sgControl, red text is sgBckdha. Blue arrows indicate a flux is decreased in sgBckdha compared to sgControl, while a red arrow indicates an increase in flux in sgBckdha. Bold text indicates significantly different reactions.

Figure 7
Acad8 deficiency impacts anaplerosis and alters OCFA and BCFA accumulation

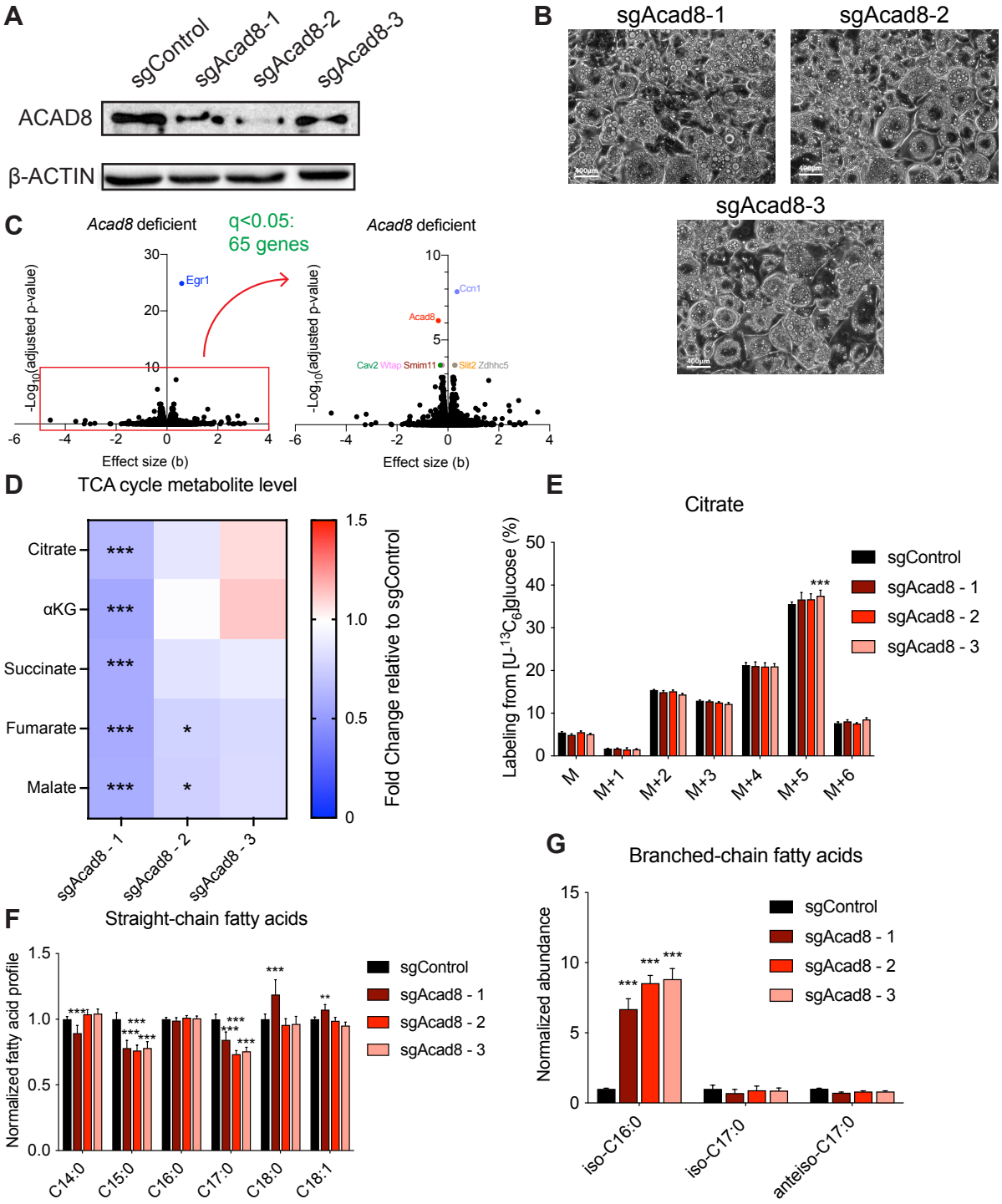

A. Western blot of Acad8 and Actin
B. Brightfield images of differentiated Control and sgAcad8 adipocytes 7 days post-induction of differentiation (scale bar = 400μm)
C. Volcano plots of differentially expressed genes in Acad8 deficient adipocytes compared to Control adipocytes
D. Heat map of the fold change of the abundance of intracellular TCA cycle intermediates in Bckdha deficient adipocytes normalized to sgControl
E. Citrate mass isotopomer distribution (MID) after 48 hours of incubation with [U-13C6]glucose
F. Relative fold change in total odd- and even- straight-chain fatty acids in Acad8 deficient 3T3-L1 adipocytes normalized to Control adipocytes.
G. Relative fold change in total branched-chain fatty acids (BCFAs) in Acad8 deficient 3T3-L1 adipocytes normalized to Control adipocytes.
Data are presented as means ± SD (E-G) with three cellular replicates. Two-way ANOVA with Dunnett's correction for multiple comparisons (E-G). Significance in all is compared to sgControl. Results are depicted from one representative experiment which was repeated independently at least three times. *p<0.05, **p<0.01, ***p<0.001.

Supplementary Figure 1
Bckdha deficiency alters BCKA levels and amino acid metabolism

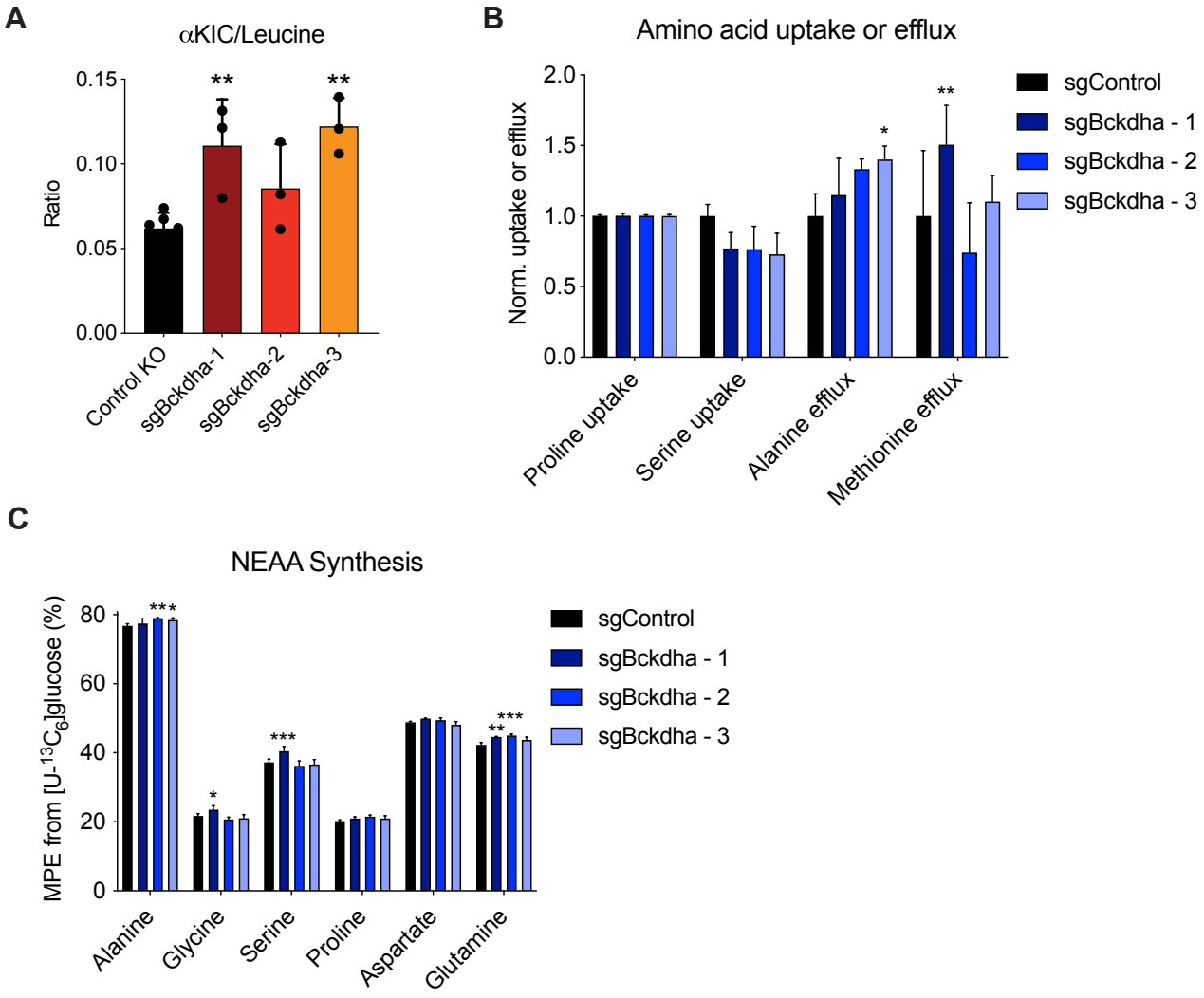

A. Ratio of α-ketoisocaproate (α-KIC) to leucine in Control and Bckdha deficient adipocytes
B. Normalized relative uptake or efflux of amino acids in Control and Bckdha deficient adipocytes
C. Mole percent enrichment (MPE) of non-essential amino acids alanine, glycine, serine, proline, aspartate, and glutamine from [U-13C6]glucose

Data are presented as means ± SD (A-C) with three cellular replicates. One-way ANOVA (A) or two-way ANOVA (B-C). Significance in all is compared to sgControl. Results are depicted from one representative experiment which was repeated independently at least three times.
*p<0.05, **p<0.01, ***p<0.001.

Supplementary Figure 2
Bckdha deficiency alters transcription and glucose metabolism without affecting mitochondrial number

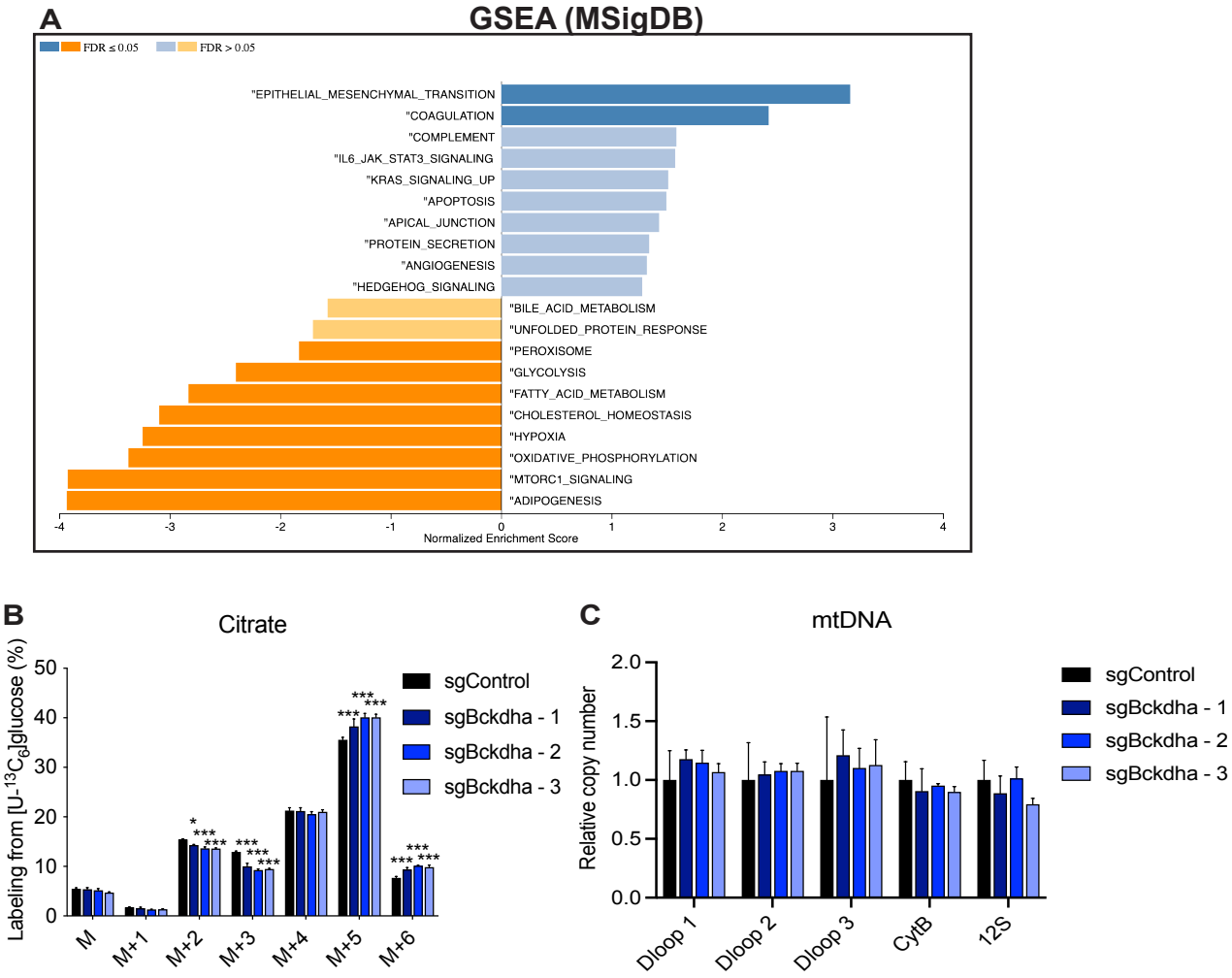

A. Gene set enrichment analysis of Bckdha deficient adipocytes generated using WEB-based GEne SeT AnaLysis Toolkit (WebGestalt) using the MsigDB biological processes hallmarks database
B. Citrate mass isotopomer distribution (MID) after 48 hours of incubation with [U-13C6]glucose
C. Normalized gene expression of mitochondrial DNA markers in Control and Bckdha deficient adipocytes

Data are presented as means ± SD (B, C) with three cellular replicates. Two-way ANOVA (B, C). Significance in all is compared to sgControl. Results are depicted from one representative experiment which was repeated independently at least three times.
*p<0.05, **p<0.01, ***p<0.001.